Programmable and Open-Access Millimeter-Wave Radios in the PAWR COSMOS Testbed

Tingjun Chen[⋆], Prasanthi Maddala[‡], Panagiotis Skrimponis[♮], Jakub Kolodziejski[‡], Xiaoxiong Gu[♯], Arun Paidimarri[♯], Sundeep Rangan[♮], Gil Zussman[†], Ivan Seskar[‡]

[⋆]Electrical and Computer Engineering, Duke University, [♮]Electrical and Computer Engineering, NYU, [♯]IBM Research, [†]Electrical Engineering, Columbia University, [‡]WINLAB, Rutgers University

ABSTRACT

While millimeter-wave (mmWave) wireless has recently gained tremendous attention with the transition to 5G, developing a broadly accessible experimental infrastructure will allow the research community to make significant progress in this area. Hence, in this paper, we present the design and implementation of various programmable and open-access 28/60 GHz software-defined radios (SDRs), deployed in the PAWR COSMOS advanced wireless testbed. These programmable mmWave radios are based on the IBM 28 GHz 64-element dual-polarized phased array antenna module (PAAM) subsystem board and the Sivers IMA 60 GHz WiGig transceiver. These front ends are integrated with USRP SDRs or Xilinx RFSoC boards, which provide baseband signal processing capabilities. Moreover, we present measurements of the TX/RX beamforming performance and example experiments (e.g., real-time channel sounding and RFNoC-based 802.11ad preamble detection), using the mmWave radios. Finally, we discuss ongoing enhancement and development efforts focusing on these radios.

CCS CONCEPTS

• **Networks** → **Network experimentation**; *Wireless access networks*; • **Hardware** → *Radio frequency and wireless circuits.*

KEYWORDS

Millimeter-wave communication; software-defined radios; wireless experimentation; COSMOS testbed

ACM Reference Format:

Tingjun Chen, Prasanthi Maddala, Panagiotis Skrimponis, Jakub Kolodziejski, Xiaoxiong Gu, Arun Paidimarri, Sundeep Rangan, Gil Zussman, Ivan Seskar. 2022. Programmable and Open-Access Millimeter-Wave Radios in the PAWR COSMOS Testbed. In *The 15th ACM Workshop on Wireless Network Testbeds, Experimental evaluation & CHaracterization (WiNTECH '21), January 31–February 4, 2022, New Orleans, LA, USA.* ACM, New York, NY, USA, 8 pages. https://doi.org/10.1145/3477086.3480834

1 INTRODUCTION

Millimeter-wave (mmWave) communication is a key technology for 5G and future wireless networks, where the widely available spectrum at mmWave frequencies can be leveraged to achieve very high data rates (above Gbps) in cellular, Wi-Fi, and wireless backhaul systems [1–3]. Such capabilities can enable a broad range of real-time applications including augmented reality and autonomous vehicles. While there has been extensive recent development and demonstrations of practical mmWave systems (e.g., [4–9]), experimentation with state-of-the-art programmable mmWave radios in real-world environments it still a major challenge for researchers from both academia and industry.

To address this challenge and to allow the broader community to conduct experiments with mmWave wireless and other state-of-the-art technologies, in [10], we presented the city-scale open-access COSMOS testbed, which is being deployed in West Harlem, New York City (NYC), as part of the NSF Platforms for Advanced Wireless Research (PAWR) program [11]. One key technological component of the COSMOS testbed is a variety of *programmable* mmWave front ends at 28/60 GHz, USRP software-defined radios (SDRs) and Xilinx RFSoC evaluation boards, as well as end-to-end mmWave systems, which can enable various experimental capabilities across different layers of the networking stack.

In this paper, we first present a brief overview of the relevant COSMOS testbed components, including the two sandboxs (`sb1` and `sb2`). Then, we present the programmable mmWave front ends and their integration with USRP SDRs and/or Xilinx RFSoC boards, which have been deployed in the COSMOS testbed. These front ends include the IBM 28 GHz 64-element dual-polarized phased array antenna module (PAAM) subsystem board [12, 13] and the Sivers IMA 60 GHz WiGig transceiver system. We also present the developed software and application program interfaces (APIs) for hardware control and experimentation. Finally, we present measurements and experiments with the 28 GHz PAAM board, which is integrated with a USRP N310, and the 60 GHz Sivers IMA transceiver, which is integrated with a USRP N310 and a Xilinx RFSoC board.

To summarize, this paper details the *design and implementation of the programmable and open-access 28/60 GHz radios, which are deployed in real-world indoor and outdoor environments and can be remotely used by the community.* These open-access hardware/software resources and example experiments can be extended to more complicated networking scenarios and facilitate experimentation with advanced mmWave technologies.

2 RELATED WORK

There has been extensive recent research on the design and development of mmWave systems and testbeds, including the X60 platform [4], M-Cube [5], mm-FLEX [6], MIMORPH [7], Pi-Radio [14], OpenMili [8], and MiRa [9], which mostly focus on 60 GHz wireless. In particular, X60 [4] is an SDR-based testbed for 60 GHz WLANs

WiNTECH '21, January 31–February 4, 2022, New Orleans, LA, USA

ACM ISBN 978-1-4503-8703-3/22/01…$15.00
https://doi.org/10.1145/3477086.3480834

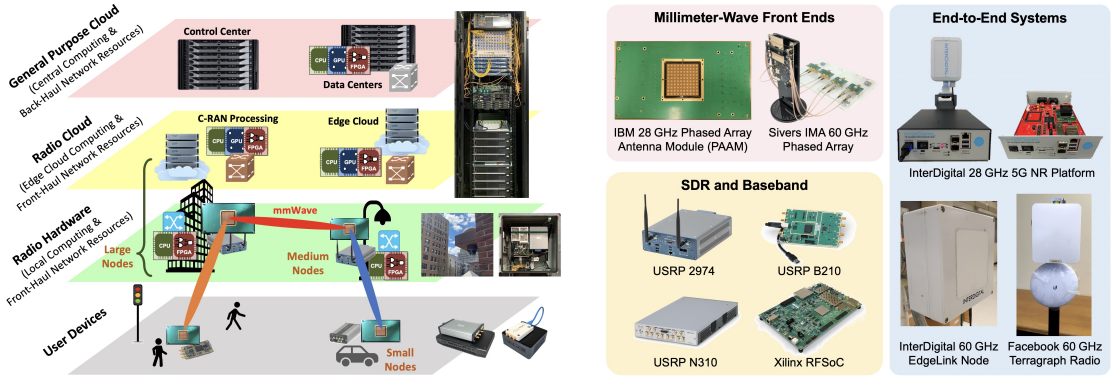

(a) (b)

Figure 1: (a) COSMOS' multi-layered computing architecture, which includes radio nodes with different form factors and computational capabilities, and (b) various millimeter-wave (mmWave) front ends and systems integrated in the COSMOS testbed and sandboxes.

using a small 12-element phased antenna array with programmable PHY/MAC/Network layers. M-Cube [5] is a 60 GHz massive MIMO SDR based on the commodity Airfide 802.11ad radio. The most relevant to COSMOS' 60 GHz SDRs is MIMORPH [7], which is a real-time experimental platform for sub-6 GHz and mmWave MIMO systems, where the Sivers IMA 60 GHz transceiver is integrated with a Xilinx RFSoC board. In addition, the PAWR POWDER-RENEW [15, 16] and AERPAW [17] testbeds have a technological focus on sub-6 GHz massive MIMO wireless and aerial communications, respectively. In comparison, COSMOS provides a broad range of programmable and open-access mmWave front ends deployed in real-world scenarios. These mmWave front ends with more advanced capabilities include the IBM 28 GHz PAAM subsystem board, whose integration with an SDR and an API as a software-defined phased array platform was described in [18].

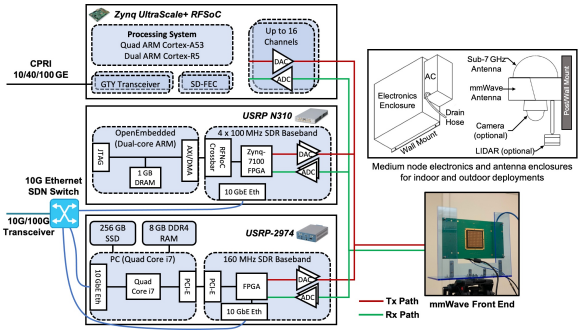

Figure 2: Example block diagram of a programmable mmWave node in COSMOS, where different configurations include a subset of the major components (e.g., the 28 GHz PAAM board with a USRP N310).

3 TESTBED, SANDBOXES, AND MMWAVE

COSMOS [10, 19] is an open-access city-scale advanced wireless testbed that is being deployed in West Harlem, NYC, as part of the NSF PAWR program [11]. Fig. 1(a) shows COSMOS' multi-layered computing and network architecture with different levels of programmability from user devices up to the edge and central cloud. In particular, there are three types of COSMOS nodes with different form factors for different deployment scenarios, which include: *large* nodes (macro cells installed on rooftops), *medium* nodes (small cells installed on building side and lightpoles), and *small* nodes (near-portable fixed or mobile devices). The deployment of COSMOS consists of three main sites: (*i*) a sandbox located in WINLAB at Rutgers University with both indoor and outdoor deployments (sb1), (*ii*) an indoor sandbox located in the CEPSR Building at Columbia University (sb2), and (*iii*) the outdoor testbed site that is currently being deployed in West Harlem, NYC (bed). The open-access nature of COSMOS allows worldwide users to remotely use the testbed and experiment with advanced wireless and edge cloud technologies. More details about the design and deployment of the COSMOS testbed, as well as extensive 28 GHz channel measurements in the testbed area, can be found in [10, 19–21].

Key technological components of COSMOS are several mmWave front end systems and radios, as shown in Fig. 1(b) and described in §4. In particular, COSMOS includes two main mmWave front end systems: (*i*) the IBM 28 GHz 64-element dual-polarized phased array antenna module (PAAM) subsystem board (§4.1), and (*ii*) the Sivers IMA 60 GHz 16-element phased array transceiver (§4.2), each of which can be attached to an SDR or a Xilinx RFSoC board to form a *programmable* mmWave radio. Fig. 2 shows an example diagram of a COSMOS node equipped with mmWave capabilities, which includes a mmWave front end system (e.g., the 28 GHz PAAM board) and an SDR (e.g., the USRP N310). It also shows the wall-mounted enclosures for node electronics and antennas for indoor and outdoor deployments, respectively. Different SDRs and compute host are selected based on the node form factor and portability requirements (§4.3). For example, an infrastructure medium node mounted on a building side with available power supply consists of a high-end USRP N310 SDR/Xilinx RFSoC board connected to the compute servers via a high-speed optical front-haul, whereas a battery-powered mobile node consists of a USRP B210/E312 SDR and an Intel NUC for data storage and processing (§4.4).

COSMOS also supports end-to-end mmWave experimentation using the 28 GHz 5G NR platform and 60 GHz EdgeLink nodes from InterDigital (§4.5), and the 60 GHz Terragraph radios from Facebook as part of the Telecom Infra Project (TIP). In this paper, we focus on the programmable mmWave front ends integrated with SDRs. More detailed information about these end-to-end systems and the relevant tutorials are available at [22, 23].

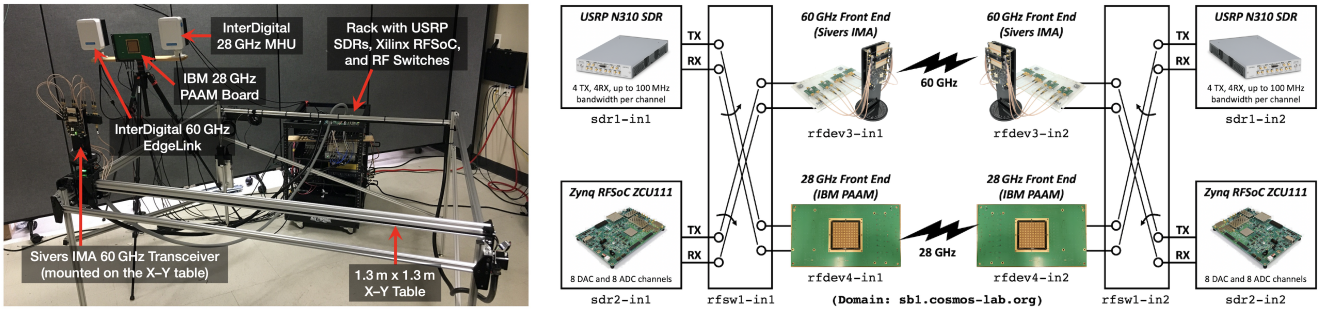

Figure 3: The COSMOS Sandbox 1 (sb1): (a) view of a corner of sb1 in an indoor environment, and (b) block diagram of the bench-top mmWave setup with programmable 28/60 GHz front end systems, customized RF switches, USRP SDRs, and Xilinx RFSoC boards.

4 PROGRAMMABLE MMWAVE RADIOS

In this section, we present the programmable mmWave radios in COSMOS and focus on the 28/60 GHz SDRs deployed in sb1 and sb2 (see Figs. 3 and 4). The indoor deployments and experimentation help drive and validate various system designs, which are important for the ongoing outdoor deployment of 28 GHz SDRs in bed.

4.1 IBM 28 GHz PAAM Subsystem Board

Fig. 4(a) shows the IBM 28 GHz 64-element dual-polarized PAAM [12, 13], which can enable a broad range of mmWave experiments with fast (e.g., sub-µs) beam steering capability and multi-beam support. An important feature of the PAAM is the use of antenna feed lines with equal delay, uniform antenna radiation patterns across the array, and orthogonal amplitude and phase control per element in the IC, which enable high-precision beam steering capability *without any calibration*. Fig. 4(b) shows the architecture diagram of a compact 28 GHz *PAAM subsystem board* reported in [24], which is a 10 in × 5.75 in printed circuit board (PCB) consisting of a 28 GHz PAAM, intermediate frequency (IF) and local oscillator (LO) splitters, IF/LO baluns, programmable switches, and an on-board phased locked loop (PLL) for LO generation.

The TX/RX interfaces of the PAAM board are at 3 GHz IF through SMP connectors, which allows for direct connection to a USRP SDR or an RFSoC board. We prototyped four 28 GHz SDRs using the PAAM boards and N310 SDRs in sb1 and sb2, as shown in Figs. 3(a) and 4(c). Using the IF switches/splitters and the 20 IF ports on the PAAM subsystem board, a broad range of SISO and MIMO mmWave configurations can be realized, which include up to 8 simultaneous 16-element independent beams in each TX/RX mode across both H-polarization and V-polarization. The PAAM subsystem board also supports the direct plug-in of an off-the-shelf Avnet MicroZed FPGA system-on-module (SoM), which supports the configuration of various subsystem features through a high-level API. Further details about the development of the PAAM board are in [24].

The software and firmware control architecture of the 28 GHz PAAM board are presented in [24]. This architecture evolved from the software-define phased array radio (SDPAR) demonstration presented in [18]. In particular, users can send high-level PAAM control commands from the host to the MicroZed via the Ethernet interface using a Python API. When the ARM processor core of the MicroZed FPGA receives the commands, it will initiate the low-level communication protocols to communicate with and configure

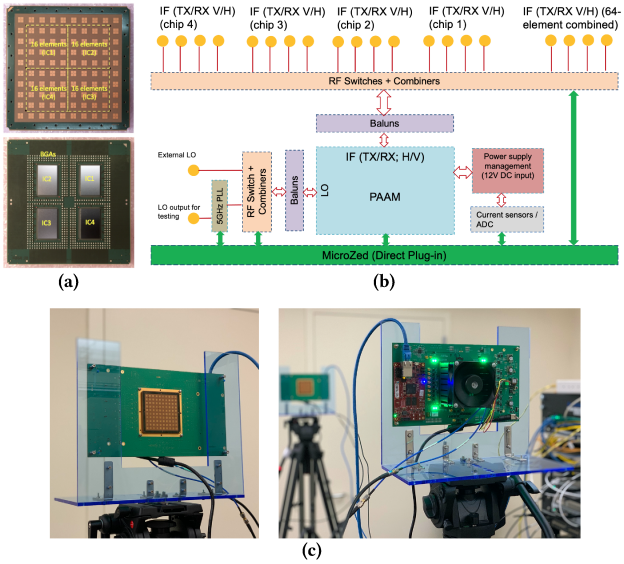

Figure 4: (a) Top/bottom view of an IBM 28 GHz PAAM [12], (b) architecture diagram of the 28 GHz PAAM subsystem board [24], and (c) two PAAM subsystem boards integrated in the COSMOS sb2.

the PAAM subsystem board. Table 1 summarizes the main board-level and IC-level functions supported by the PAAM board and the software API, which are responsible for configuring the PAAM board (e.g., PLL for on-board LO generation and IF switches) and the PAAM itself (e.g., TX/RX mode of operation, H/V-polarization, number of activated front end elements, and control of beamforming). In §5, we present measurements and example experiments using the PAAM boards integrated with USRP N310 SDRs, using the developed API.

4.2 Sivers IMA 60 GHz WiGig Transceiver

Another supported mmWave front end is the Sivers IMA 57–66 GHz WiGig transceiver system, which is optimized for high performance WiGig applications and is compliant with the IEEE 802.11ad standard. This transceiver, which was also used in [6, 7], includes two integrated 16-element patch antenna arrays for TX and RX, and supports beam steering capabilities using an application GUI or a Python API over the USB interface. We connect the Sivers IMA transceiver with COTS baluns to convert its differential TX input

Table 1: Main board-level and IC-level functions supported by the PAAM subsystem board and software API.

PAAM API Command	Function
Board-level functions for the PAAM subsystem board object, `paam_board`	
`paam_board.set_lo_switch(bool external)`	Set the LO switch to use an external LO source or the on-board PLL
`paam_board.pll_init()`	Initialize and set the on-board PLL (use only with `set_lo_switch(external=False)`)
`paam_board.set_if_tx_h(bool combine)`	Set the IF TX input in H-polarization to combined (across 4 ICs) or separate (individual IC)
`paam_board.set_if_tx_v(bool combine)`	Set the IF TX input in V-polarization to combined (across 4 ICs) or separate (individual IC)
`paam_board.set_if_rx_h(bool combine)`	Set the IF RX output in H-polarization to combined (across 4 ICs) or separate (individual IC)
`paam_board.set_if_rx_v(bool combine)`	Set the IF RX output in V-polarization to combined (across 4 ICs) or separate (individual IC)
`paam_board.get_adc_vals()`	Read values from the 12 ADC channels including the current consumption of individual ICs and the entire PAAM board
IC-level functions for the PAAM object, `paam`	
`paam.enable(ic,fe_list,txrx,pol)`	Enable and configure a set of front end elements (`fe_list`) for a given IC (`ic`), TX/RX mode (`txrx`), and polarization (`pol`)
`paam.steer_beam(ics,txrx,pol,theta,phi)`	Steer the beam to a given direction (`theta, phi`) for a given set of ICs (`ics`), TX/RX mode (`txrx`), and polarization (`pol`)
`paam.set_arbitrary_beam(ics,txrx,pol,gains,phases)`	Set arbitrary beam patterns by setting the phase and gain for each individual front end element
`paam.switch_beam_index(ic,txrx,pol,beam_index)`	Switch to the pre-recorded beam index (`beam_index`) for a given IC (`ic`), TX/RX mode (`txrx`), and polarization (`pol`)
`paam.switch_beam_indexes(ic,txrx,beam_index_h,beam_index_h)`	Switch to the pre-recorded beam indexes in both H-polarization and V-polarization simultaneously (`beam_index_h` and `beam_index_v`) for a given IC (`ic`) and TX/RX mode (`txrx`)

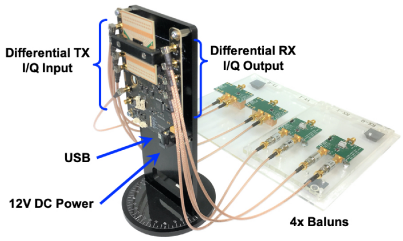

Figure 5: The Sivers IMA 60 GHz WiGig transceiver with baluns.

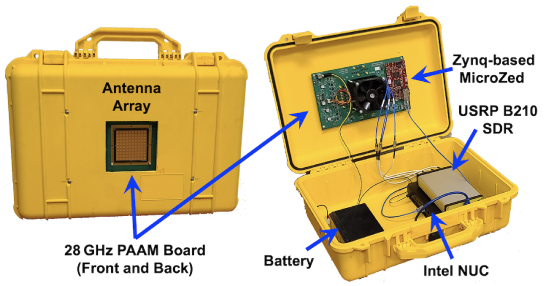

Figure 6: A programmable mobile 28 GHz SDR using the PAAM board: the waterproof enclosure and internal component layout.

and RX output ports to single-ended ports (see Fig. 5), which are further connected to a USRP SDR or a Xilinx RFSoC board to form a 60 GHz SDR. In §6, we present experiments using the Sivers 60 GHz transceiver with both a USRP N310 SDR and an RFSoC board, as shown in Figs. 3(a) and 3(b).

4.3 USRP SDRs, RFNoC, and Xilinx RFSoC

USRP SDRs and RFNoC: In general, SDRs are used for baseband processing for radios operating in both sub-6 GHz and mmWave frequencies. COSMOS' programmable mmWave radios use the USRP 2974/N310/B210 SDRs and/or the Xilinx RFSoC boards for high-bandwidth data streaming and processing. In particular, the USRP-2974 and N310 SDRs are equipped with on-board CPUs and can be used in stand-alone mode or in conjunction with a host server. The two 10 GbE SFP+ ports on the USRP-2974 and N310 are connected to COSMOS' data networks, allowing for high-speed data transfer between the SDR and host server. Both USRP-2974 and N310 SDRs support the RFNoC development framework, which leverages the resource dense FPGAs for real-time signal processing.

RFNoC is a unique processing and routing architecture for 3rd-generation USRP devices, which reduces the FPGA development time by providing basic SDR functionalities (e.g., host communication, radio interfaces, and clocking) while allowing users to easily integrate custom IP. It also allows for dynamic composition of flow-graphs by connecting various FPGA modules at run-time. Attaching mmWave front ends to RFNoC-enabled USRP SDRs in COSMOS allows users to offload computationally intensive and time-sensitive tasks to the FPGA in a mixed hardware-software design.

Xilinx RFSoC Board (ZCU111): The core processing of an RFSoC-based SDR is a ZCU111 evaluation board featuring a Xilinx Zynq UltraScale+ ZU28DR RFSoC FPGA, a quad-core ARM Cortex-A53 processing system and a dual-core ARM Cortex-R5 real-time processor, 8 high-speed 14-bit DACs and 12-bit ADCs, and several high-speed gigabit transceiver ports. Another highlight of this board is the soft-decision forward error correction (SD-FEC) cores in silicon, which are used to implement highly computational codes (e.g., Turbo, LDPC, Polar) without using any FPGA resources.

For real-time experimentation, we exploit the USRP hardware driver (UHD), which is targeted mainly at the USRP devices. Similarly to USRP SDRs, the ZCU111 board is also addressable through a 1 GbE connection and allows for access to the embedded Linux system. The host can access the ZCU111 board through a network RPC-based API and communicate with the module peripheral manager daemon. For applications requiring high data rates, four 10 GHz SFP+ interfaces on the ZCU111 board can be used. Using the Xilinx Vivado tool and open-embedded Linux tools, we modified the open-source files of UHD 3.13 to target the ZCU111. Such a unified software interface allows seamless transition between different applications, and any software supporting a UHD device (i.e., GNU Radio) can be used to control the ZCU111. For non-real-time experimentation (see §6), we utilize the 1/10/25 GbE interface to connect the ZCU111 with a host server over TCP/IP. The host drivers are implemented in both Python and MATLAB, enabling a wide range of experiments. The TX data can be generated and pre-stored in a BRAM, and the RX data can be collected in continuous or burst mode and stored in the PL-DDR for post processing.

For RF front ends supporting multiple channels such as the IBM 28 GHz PAAM board and the Sivers IMA 60 GHz WiGig transceiver, the ZCU111 board also supports multi-tile synchronization (MTS) of the RF data-converter Xilinx IP. The RFSoC reads signals either in baseband or in RF utilizing a numerically controlled oscillator

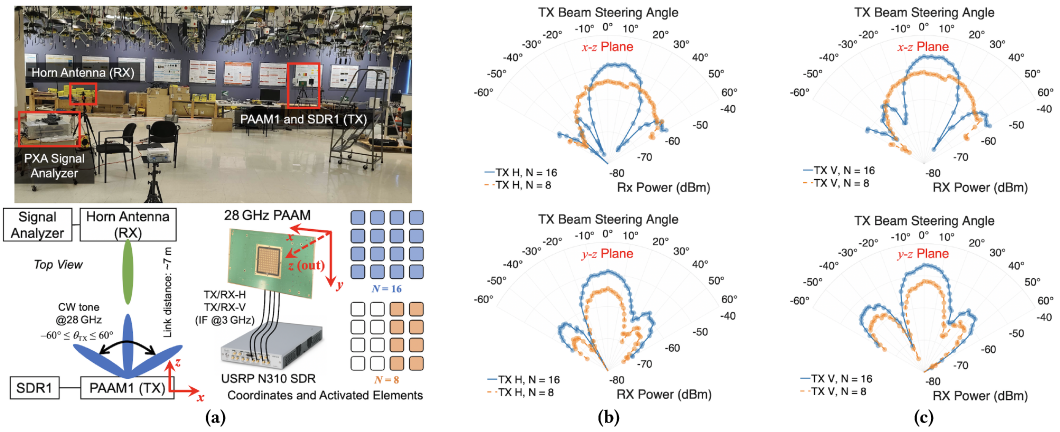

Figure 7: (a) Setup for the TX beamforming measurements using the 28 GHz PAAM subsystem board in COSMOS sb1, which include a 28 GHz PAAM board, a USRP N310 SDR, a standard gain horn antenna, and a Keysight PXA signal analyzer. (b)–(c) Measured received signal power at the horn antenna with varying TX beam steering angles at the PAAM in the x-z and y-z plane, and in H- and V-polarization.

(NCO) to downconvert them and generate the corresponding I/Q waveforms. While the base sampling rate is at 3932.16 MHz in the MTS mode, the internal interpolation/decimation structure can be explored to reduce the bandwidth, if needed.

4.4 Mobile 28 GHz SDRs

To support experiments in mobile scenarios within the COSMOS testbed area, we also build a mobile 28 GHz SDR using the PAAM subsystem board described in §4.1 and [24]. Fig. 6 shows the waterproof enclosure and internals of the mobile 28 GHz SDR, which includes a 28 GHz PAAM subsystem board, a USRP B210 SDR, an Intel "Hades Canyon" NUC, and a sealed lead acid (SLA) battery. In particular, the USRP B210 is equipped with 2 TX and 2 RX, which are connected to the TX-H/TX-V and RX-H/RX-V IF ports of the PAAM subsystem board, respectively, and supports a real-time RF bandwidth of up to 56 MHz via the USB3 interface. In future work, we will consider replacing the USRP B210 SDR with a USRP X410 SDR or an RFSoC board, which can support 4 TX-RX pairs with a higher real-time bandwidth. Using such a capability, researchers can perform various experiments in mobile scenarios, where a user moving on the street (i.e., the compact mobile 28 GHz SDR) communicates with a fixed infrastructure node (e.g., a medium node equipped with the 28 GHz PAAM subsystem board).

4.5 InterDigital mmWave Systems

COSMOS sb1 also includes the InterDigital 5G NR platform and EdgeLink radios, as shown in Fig. 1(b). In particular, the 5G NR platform is an NR Rel-15 28 GHz radio with a 64-element phased array and a Xilinx MPSoC-based processing unit in the baseband. EdgeLink is a 60 GHz wireless link solution based on the IEEE 802.11ad standard, which supports mmWave mesh transport technology with a centrally controlled mesh software. Detailed information and example tutorials can be found at [23].

5 EXPERIMENTATION WITH THE 28 GHZ PAAM SUBSYSTEM BOARD

In this section, we present extensive measurements and an example channel sounding experiment using the 28 GHz PAAM subsystem boards integrated with USRP N310 SDRs in the indoor COSMOS sb1 and sb2, as shown in Figs. 3 and 4(c). In particular, the IF TX/RX ports in both the H-polarization and V-polarization on IC0 of a PAAM subsystem board are connected to two transceiver pairs on the N310 SDR (RF2 and RF3). We choose to use only one IC on the PAAM (IC0) with up to 16 front end elements, due to the short link distances of up to 70 feet in sb1. However, the ongoing outdoor deployment of the 28 GHz subsystem boards in bed will support up to 64-element dual-polarized beamforming using all the 4 ICs, which can result in a link distance of 100s of meters. The experimental results presented below can also be applied to the mobile 28 GHz SDR described in §4.4, where the real-time bandwidth will be limited by the Intel NUC and USRP B210 SDR.

5.1 TX Beamforming

Fig. 7(a) shows the experimental setup for TX beamforming performance measurement, where the TX is a 28 GHz PAAM board integrated with a USRP N310 (PAAM1 and SDR1), and the RX is an SAS-588 standard gain horn antenna connected to a Keysight N9030A PXA signal analyzer. The PAAM board and RX horn antenna, which face each other (roughly) in the broadside, are mounted on two tripods with the same height and the link distance between them is ~7 meters. In particular, the N310 SDR generates a 100 kHz continuous wave (CW) at 3 GHz operating frequency and sends it to the IF TX input port of IC0 on the PAAM board, in the H-polarization or V-polarization. The PXA signal analyzer is configured with a center frequency of 28 GHz and a resolution bandwidth (RBW) of 10 kHz in order to capture received signal with low power levels, and the average RX signal power is recorded. We perform measurements of the TX beamforming performance of the PAAM in both the H-polarization and V-polarization, where the RX horn antenna is set up such that its polarization matches with that of the PAAM.

Figs. 7(b) and 7(c) show the measured RX power as a function of the TX beam steering angle in the H-polarization and V-polarization, respectively. In general, the TX beamforming performance is largely similar between the H-polarization and V-polarization. For each polarization, the RX power at the horn antenna is measured when the TX beam is swept across the x-z or y-z plane (see Fig. 7(a) for

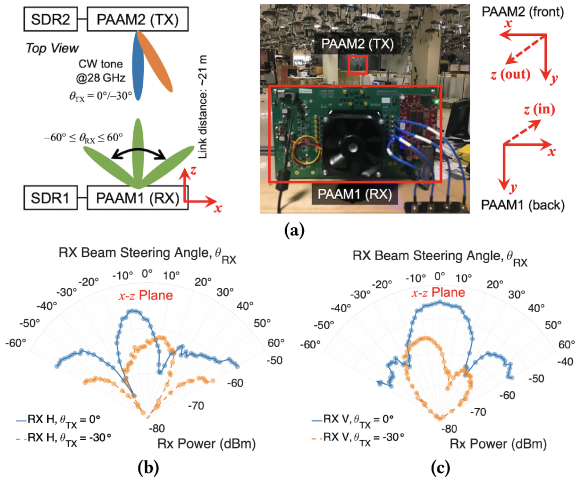

Figure 8: (a) Setup for the RX beamforming measurements in COSMOS sb1, which includes two 28 GHz PAAM boards and two USRP N310 SDRs. (b)–(c) Measured received signal power with varying RX beam steering angles on the x-z plane in H- and V-polarization.

the coordinate system of the PAAM subsystem board), with 8 or 16 front end elements activated on IC0. The results show a clear beam shape as the TX beam is electronically steered using the developed PAAM API. With 16 antenna elements, a peak-to-null radio of >30 dB and an average half-power beamwidth of 26° are measured in the indoor environment of sb1. With only 8 front end elements being activated on IC0, the peak power is reduced by ~6 dB compared with the case with 16 front end elements. In addition, the half-power beamwidths on the x-z and y-z planes exhibit a large difference, due to the asymmetric number of elements on the x and y axes with 8 front end elements. Note that these results *do not* show the standard TX beam pattern measurements, since the PAAM or the RX horn antenna is not mechanically rotated for each fixed TX beamforming direction.[1] However, the reported measurements are still valuable as a demonstration of the practical remote usage of various hardware/software resources in sb1 with over-the-air signal transmissions. Our ongoing work includes careful measurements of the TX/RX beam patterns in an anechoic chamber and their cross-comparison with that reported in [12, 13], and the measurement datasets will be made available on the COSMOS wiki for the experimenters' reference.

5.2 RX Beamforming

We also conduct RX beamforming performance measurements and the experimental setup is shown in Fig. 8(a), where PAAM1 used in the TX beamforming measurements, described above, is configured in the RX mode, and another PAAM board with a USRP N310 (PAAM2 and SDR2) is used as the TX. On the TX side, we configure PAAM2 to form a 16-element TX beam in two directions ($\theta_{TX} = 0°/-30°$) on the x-z plane, and set SDR2 to generate a 100 kHz CW at 3 GHz carrier frequency, which is sent to the IF TX input port of IC0 on PAAM2. On the RX side, PAAM2 is configured to form a 16-element RX beam in the x-z plane, and the received signal power at SDR2 with varying RX beamforming directions is recorded.

[1]The detailed setup and measurement results of the true TX/RX beam patterns in an antenna chamber are presented in [12].

Table 2: Timing of the IC-level functions supported by the PAAM board and software API using a single IC.

PAAM API Command	$f_{\text{MicroZed}} = 10$ MHz	$f_{\text{MicroZed}} = 50$ MHz
`enable()`[(i)]	<27.0 µs	<5.4 µs
`steer_beam()`[(i)]	<39.6 µs	<7.92 µs
`set_arbitrary_beam()`[(i)]	<39.6 µs	<7.92 µs
`switch_beam_index()`	1.2 µs	0.24 µs
`switch_beam_indexes()`	1.2 µs	0.24 µs

[(i)] Running time depends on the number of used front end elements.

Figs. 8(b) and 8(c) show the measured RX power as a function of the RX beam steering angle, θ_{RX}, in the H-polarization and V-polarization, respectively. The results show that the maximum RX signal power in the V-polarization is ~10 dB higher than that in the H-polarization in the sb1 indoor environment. This is due to the spatial dimension of sb1 (see Figs. 7(a) and 8(a)), which is an indoor environment with a dimension of 20 m × 20 m × 3 m (L × W × H). When the signal propagates on the y-z plane (V-polarization), its energy is "trapped" between the ceiling and ground, resulting in a higher RX power level compared with the H-polarization. Similar effects stemming from the sb1 indoor environment can also be seen by the strong RX signal power in the H-polarization at $\theta_{RX} = \pm 60°$ on the x-z plane. In practice, a smaller number of front end elements (e.g., 4 or 8) on the TX and RX side can already form a link with sufficient signal-to-noise ratio (SNR) at ~70 feet distance. However, we perform measurements using 16-element TX and RX beams with a narrower half-power beamwidth in order to quantify the spatial distribution of the RX signal power levels.

5.3 Timing of the PAAM API Functions

We now present experimental evaluations of the timing of the main IC-level PAAM functions, described in Table 1, using the same setup described in §5.2, and the main results are summarized in Table 2.

Beam Steering/Switching: To experimentally measure the beam steering/switching time, we configure PAAM1 (RX) to form a 16-element RX beam in the broadside, and configure PAAM2 (TX) to generate a 16-element TX beam and continuously switch between two TX beamforming directions, $\theta_{TX} = 0°$ and $\theta_{TX} = 30°$. Figs. 9(a) and 9(b) show the RX signal power at PAAM1 when PAAM2 employs the `steer_beam()` and `switch_beam_index()` functions, respectively. The results show that by computing and storing the beamforming codebook in advance, the `switch_beam_index()` function can improve the beam switching time by a factor of 10× compared to the `steer_beam()` function, which computes the codebook every time a beamforming direction is given. Overall, with a MicroZed frequency of 50 MHz, the `switch_beam_index()` function enables extremely fast beam switching at a speed of only 0.24 µs. This duration is much shorter than the OFDM symbol duration for 5G NR in the frequency range 2 (FR2), which is usually at the order of 10s of µs. As a result, the PAAM board can support symbol-level beam switching for practical 28 GHz systems. Note that here we report the command execution time on the MicroZed, which excludes the host-to-MicroZed latency (which is ~80 ms in sb1 and sb2). However, this can be resolved by pre-recording and replaying long sequences of commands in the Microzed.

TX-RX Switching: Using a similar approach, we perform measurements to characterize the timing of the TX-RX switching (i.e., TX→RX or RX→TX) operation using the PAAM, which is a critical

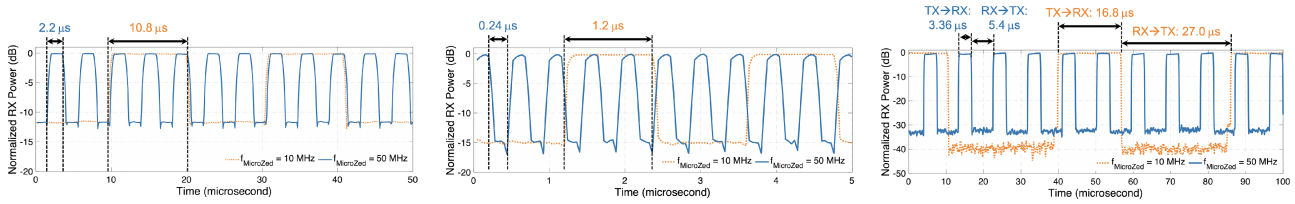

(a) The `steer_beam()` function (b) The `switch_beam_index()` function (c) TX-RX switching

Figure 9: (a)–(b) Measured time to switch between two TX beams on the x-z plane ($\theta_{TX} = 0°$ and $\theta_{TX} = 30°$), and (c) measured time to switch between the TX and RX modes using 16 front end elements of an IC on the PAAM.

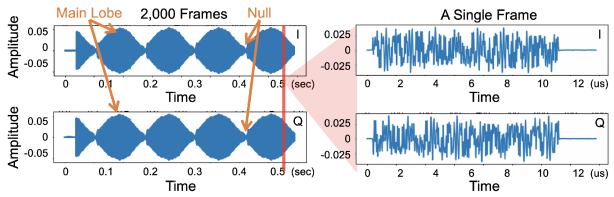

Figure 10: Baseband I/Q waveforms of a real-time 28 GHz SISO channel sounding demonstration with TX beam switching.

functionality for many time division duplex (TDD) systems. In particular, we configure PAAM2 to continuously switch between TX and RX mode with all the 16 elements on IC0 enabled, where each switching operation is realized using two functions executed in a sequencial order: `enable()`, which enables the TX/RX mode, followed by `switch_beam_index()`, which sets the TX/RX beamforming direction. On the other side, we configure PAAM1 to form a fixed 16-element RX beam in the broadside. Fig. 9(c) shows the average RX signal power at PAAM1 as a function of time, from which the TX-RX switching, performed at PAAM2, can be observed. The results show that at the maximum MicroZed clock frequency of 50 MHz, the duration to perform a TX→RX and RX→TX switching operation is 3.36 µs and 5.40 µs, respectively. Since the `switch_beam_index()` function takes minimum amount time (i.e., only 0.24 us as shown in Fig. 9(b)), the major timing overhead during a TX-RX switching operation results from the execution of the `enable()` function, which increases as more front end elements need to be switched on/off and is different for TX and RX modes.

5.4 A 28 GHz Channel Sounding Experiment

We also present a 28 GHz channel sounding experiment using two PAAM boards integrated with N310 SDRs in `sb2`, with a real-time bandwidth of 62.5 MHz. In particular, we configure one PAAM board and an N310 SDR to emulate a client, which generates a 8-element beam in the broadside in the H-polarization, and continuously sends a known sounding pilot sequence on the uplink. We configure the other PAAM board and an N310 SDR to emulate a base station, which continuously sweeps an 8-element RX beam on its x-z plane within $\theta_{RX} \in [-30°, 30°]$ in the H-polarization, using the `steer_beam_index()` method running at 2 ms time interval. The software for this experiment is built on the open-source C++-based RENEW channel sounder [25], which we have enhanced to support UHD-based SDRs. Fig. 10 shows the I/Q waveforms of the uplink pilot received at the base station, where the amplitude of the RX signal varies in proportion to the RX beam steering directions. Further channel sounding information can be obtained by analyzing the I/Q waveforms, and the details can be found in [23].

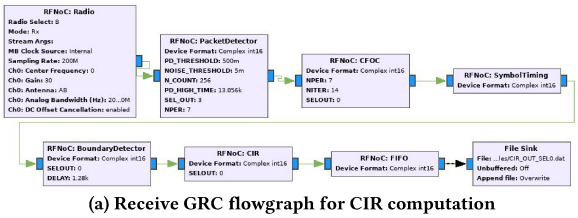

(a) Receive GRC flowgraph for CIR computation

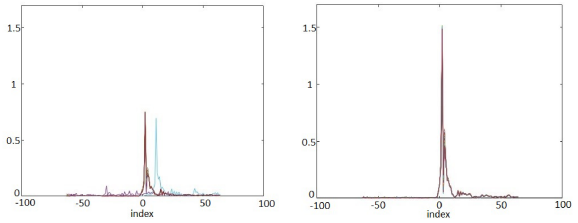

(b) CIR with TX beam angle 0^o (c) CIR with TX beam angle -5^o

Figure 11: An example experiment on RFNoC-based 802.11ad preamble processing in COSMOS `sb1`.

More advanced mmWave experiments using the PAAM boards are under development and will be made open-source once available.

6 EXPERIMENTATION WITH THE SIVERS IMA 60 GHZ TRANSCEIVER

CIR Computation using 802.11ad Preamble: We first present an experiment that uses RFNoC blocks to obtain the real-time channel impulse response (CIR) at 60 GHz using the 802.11ad preamble. Fig. 11(a) shows the GNU Radio flowgraph consisting of several RFNoC blocks: packet detector, carrier frequency offset (CFO) estimation and correction, symbol timing estimator, and frame boundary detector. These blocks were developed by IMDEA Networks Institute for the EU ORCA project [26]. We use the Sivers IMA 60 GHz transceivers integrated with USRP N310 SDRs in `sb1` (see Figs. 3(a) and 3(b)), and two host servers to control the Sivers transceiver and execute the GNU Radio RFNoC flowgraph. Pre-generated 802.11ad frames are repeatedly streamed from the TX, and the real-time CIR is obtained at the RX N310 that runs the 802.11ad preamble flowgraph. Figs. 11(b) and 11(c) show the magnitude of the CIR with two different TX beam steering angles. In particular, the RFNoC blocks compute the cross-correlation of the received channel estimation field (CEF) of the preamble with a local known sequence, with an offset between $[-63, 64]$, and an offset with index 0 corresponding to the line-of-sight direct path between the TX and RX.

Over-the-Air Transmission using RFSoC: We also developed an example experiment with over-the-air signal transmission using the RFSoC board with the Sivers IMA 60 GHz front end in `sb1`.

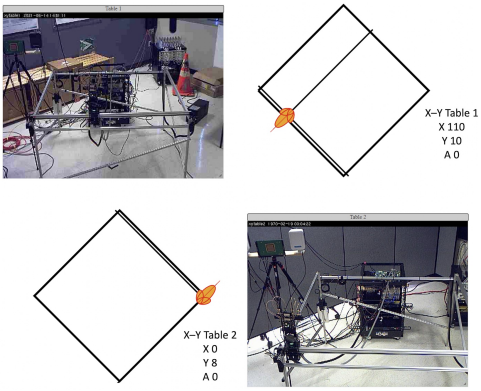

Figure 12: Web interface (including live camera streaming) for controlling the X-Y table, on which mmWave front ends are mounted.

Using the developed non-real-time library and API described in §4.3, users can send data to the DACs, receive data from the ADCs, and configure operating frequency and TX/RX beam steering directions. The received and stored data can then be processed in an online or offline manner. The detailed tutorial can be found in [23].

X-Y Table for Positioning and Orientation: Another experimental hardware in `sb1` is an X-Y table, which currently mounts the Sivers IMA 60 GHz transceiver (see Fig. 3(a)). The X-Y table allows for independent movement of each mmWave front end in the horizontal plane within a 1.3 m × 1.3 m area, and rotating the arrays within ±45° about their vertical axis. Fig. 12 shows a customized JavaScript-based web interface for controlling the position and angle of the mounted arrays, which embeds the live camera streaming functionality so that users can monitor the X-Y table remotely.

7 CONCLUSION

In this paper, we presented the design and implementation of programmable and open-access mmWave radios based on the IBM 28 GHz PAAM subsystem board and the Sivers IMA 60 GHz transceiver system. We also presented their integration in the COSMOS testbed and the associated measurements and experimentation. Our ongoing development include more advanced software (both host- and FPGA-based) for mmWave experiments at different networking layers, and the support of mmWave MIMO communication. We also anticipate that with the ongoing outdoor deployment of the IBM 28 GHz PAAM subsystem boards, more complex mmWave experiments in both static and mobile scenarios will be enabled.

ACKNOWLEDGMENTS

This work was supported in part by NSF grants CNS-1827923, OAC-2029295, AST-2037845, CNS-1836901, CNS-1302336, CCF-1564142, CNS-1547332, and ECCS-1824434, NSF-BSF grant CNS-1910757, a Google Research Scholar Award, an IBM Faculty Award, the Semiconductor Research Corporation, the industrial affiliates of NYU WIRELESS, and the PAWR Industry Consortium. We also thank Alberto Valdes-Garcia, Bodhisatwa Sadhu, and Stanislav Lukashov from IBM Research for their contributions to this project.

REFERENCES

[1] Theodore S Rappaport, Shu Sun, Rimma Mayzus, Hang Zhao, Yaniv Azar, Kevin Wang, George N Wong, Jocelyn K Schulz, Mathew Samimi, and Felix Gutierrez. Millimeter-wave mobile communications for 5G cellular: It will work! *IEEE Access*, 1:335–349, 2013.

[2] Thomas Nitsche, Carlos Cordeiro, Adriana B Flores, Edward W Knightly, Eldad Perahia, and Joerg C Widmer. IEEE 802.11ad: directional 60GHz communication for multi-gigabit-per-second Wi-Fi. *IEEE Commun. Mag.*, 52(12), 2014.

[3] Marco Giordani, Michele Polese, Marco Mezzavilla, Sundeep Rangan, and Michele Zorzi. Toward 6G networks: Use cases and technologies. *IEEE Commun. Mag.*, 58(3):55–61, 2020.

[4] Swetank Kumar Saha, Yasaman Ghasempour, Muhammad Kumail Haider, Tariq Siddiqui, Paulo De Melo, Neerad Somanchi, Luke Zakrajsek, Arjun Singh, Roshan Shyamsunder, Owen Torres, et al. X60: A programmable testbed for wideband 60 GHz WLANs with phased arrays. *Computer Communications*, 133:77–88, 2019.

[5] Renjie Zhao, Timothy Woodford, Teng Wei, Kun Qian, and Xinyu Zhang. M-Cube: A millimeter-wave massive MIMO software radio. In *Proc. ACM MobiCom'20*, 2020.

[6] Jesus Omar Lacruz, Dolores Garcia, Pablo Jiménez Mateo, Joan Palacios, and Joerg Widmer. mm-FLEX: an open platform for millimeter-wave mobile full-bandwidth experimentation. In *Proc. ACM MobiSys'20*, 2020.

[7] Jesus Lacruz, Rafael Ortiz, and Joerg Widmer. A real-time experimentation platform for sub-6 GHz and millimeter-wave MIMO systems. In *Proc. ACM MobiSys'21*, 2021.

[8] Jialiang Zhang, Xinyu Zhang, Pushkar Kulkarni, and Parameswaran Ramanathan. OpenMili: A 60 GHz software radio platform with a reconfigurable phased-array antenna. In *Proc. ACM MobiCom'16*, 2016.

[9] Omid Abari, Haitham Hassanieh, Michael Rodreguiz, and Dina Katabi. Poster: A millimeter wave software defined radio platform with phased arrays. In *Proc. ACM MobiCom'16*, 2016.

[10] Dipankar Raychaudhuri, Ivan Seskar, Gil Zussman, Thanasis Korakis, Dan Kilper, Tingjun Chen, Jakub Kolodziejski, Michael Sherman, Zoran Kostic, Xiaoxiong Gu, Harish Krishnaswamy, Sumit Maheshwari, Panagiotis Skrimponis, and Craig Gutterman. Challenge: COSMOS: A city-scale programmable testbed for experimentation with advanced wireless. In *Proc. ACM MobiCom'20*, 2020.

[11] Platforms for advanced wireless research (PAWR). https://www.advancedwireless.org/, 2021.

[12] Bodhisatwa Sadhu, Yahya Tousi, Joakim Hallin, Stefan Sahl, Scott K Reynolds, Örjan Renström, Kristoffer Sjögren, Olov Haapalahti, Nadav Mazor, Bo Bokinge, et al. A 28-GHz 32-element TRX phased-array IC with concurrent dual-polarized operation and orthogonal phase and gain control for 5G communications. *IEEE J. Solid-State Circuits*, 52(12):3373–3391, 2017.

[13] Xiaoxiong Gu, Duixian Liu, Christian Baks, Ola Tageman, Bodhisatwa Sadhu, Joakim Hallin, Leonard Rexberg, Pritish Parida, Young Kwark, and Alberto Valdes-Garcia. Development, implementation, and characterization of a 64-element dual-polarized phased-array antenna module for 28-GHz high-speed data communications. *IEEE Trans. Microw. Theory Techn*, 67(7):2975–2984, 2019.

[14] Aditya Dhananjay, Kai Zheng, Marco Mezzavilla, Dennis Shasha, and Sundeep Rangan. Fully-digital beamforming demonstration with Pi-Radio mmWave SDR platform. In *Proc. ACM MobiHoc'20*, 2020.

[15] POWDER: Platform for open wireless data-driven experimental research. https://powderwireless.net/.

[16] RENEW: Reconfigurable eco-system for next-generation end-to-end wireless. https://renew.rice.edu/.

[17] AERPAW: Aerial experimentation and research platform for advanced wireless. https://aerpaw.org/.

[18] Bodhisatwa Sadhu, Arun Paidimarri, Mark Ferriss, Mark Yeck, Xiaoxiong Gu, and Alberto Valdes-Garcia. A 128-element dual-polarized software-defined phased array radio for mm-wave 5G experimentation. In *Proc. ACM mmNets'18*, 2018.

[19] Cloud enhanced open software defined mobile wireless testbed for city-scale deployment (COSMOS). https://cosmos-lab.org/, 2021.

[20] Tingjun Chen, Manav Kohli, Tianyi Dai, Angel Daniel Estigarribia, Dmitry Chizhik, Jinfeng Du, Rodolfo Feick, Reinaldo A Valenzuela, and Gil Zussman. 28 GHz channel measurements in the COSMOS testbed deployment area. In *Proc. ACM mmNets'19*, 2019.

[21] Jinfeng Du, Dmitry Chizhik, Reinaldo A Valenzuela, Rodolfo Feick, Guillermo Castro, Mauricio Rodriguez, Tingjun Chen, Manav Kohli, and Gil Zussman. Directional measurements in urban street canyons from macro rooftop sites at 28 GHz for 90% outdoor coverage. *IEEE Trans. Antennas Propag.*, 69(6):3459–3469, 2020.

[22] COSMOS wiki. https://wiki.cosmos-lab.org/wiki/, 2021.

[23] COSMOS tutorials. https://wiki.cosmos-lab.org/wiki/tutorials/, 2021.

[24] Xiaoxiong Gu, Arun Paidimarri, Bodhisatwa Sadhu, Christian Baks, Stanislav Lukashov, Mark Yeck, Young Kwark, Tingjun Chen, Gil Zussman, Ivan Seskar, and Alberto Valdes-Garcia. Development of a compact 28-GHz software-defined phased array for a city-scale wireless research testbed. In *Proc. IEEE IMS'21*, 2021.

[25] RENEWLab: An open-source software toolbox for the RENEW massive mimo platform. https://github.com/renew-wireless/RENEWLab, 2021.

[26] ORCA MISO webpage. https://www.orca-project.eu/millimeter-wave-open-experimentation-platform/, 2021.